

Article

Trace Element and Stable Isotope Geochemistry of Lwamondo and Zebediela Kaolins, Limpopo Province, South Africa: Implication for Paleoenvironmental Reconstruction

Avhatakali Raphalalani ¹, Georges-Ivo Ekosse ^{2,*}, John Odiyo ¹, Jason Ogola ¹ and Nenita Bukalo ¹

¹ School of Environmental Sciences, University of Venda, Thohoyandou 0950, Limpopo Province, South Africa; raphalalani.avhatakali@gmail.com (A.R.); john.odiyo@univen.ac.za (J.O.); Jason.Ogola@univen.ac.za (J.O.); nenitabukalo@gmail.com (N.B.)

² Directorate of Research and Innovation, University of Venda, Thohoyandou 0950, Limpopo Province, South Africa

* Correspondence: ekosse@gmail.com; Tel.: +27-159-628-504

Received: 6 December 2018; Accepted: 31 January 2019; Published: 4 February 2019



Abstract: The aim of the present study was the paleoenvironmental reconstruction of the prevailing environment under which the Lwamondo and Zebediela kaolin deposits were formed. Hence, this study reports deuterium and oxygen stable isotope values and trace and rare earth element concentrations for two samples of kaolin. Upper continental crust-normalised trace-element patterns reveal that large ion lithophile elements and high-field-strength elements are generally depleted in Lwamondo and Zebediela kaolins, whereas transition trace elements are generally enriched in these kaolins. Upper continental crust-normalised rare earth element (REE) patterns show that there is a slight enrichment of heavy REEs (HREEs) compared to light REEs (LREEs) in these kaolins. The $\delta^{18}\text{O}$ and δD stable isotope values for kaolinite from Lwamondo ranged from 17.4‰ to 19.1‰ and from -54‰ to 84‰ , respectively, whereas those values for kaolinite from Zebediela varied from 15.6‰ to 17.7‰ and from -61‰ to -68‰ for $\delta^{18}\text{O}$ and δD , respectively. The REE patterns and the content of other trace elements indicate ongoing kaolinitisation in the Lwamondo and Zebediela kaolins with minimum mineral sorting. The sources of the kaolins varied from basic to acidic and these were derived from an active margin tectonic setting. Lwamondo kaolin was deposited in an oxic environment whereas Zebediela kaolin was deposited under suboxic/anoxic conditions. Based on the $\delta^{18}\text{O}$ and δD values of the kaolinite, they formed in a supergene environment at temperatures generally below $40\text{ }^{\circ}\text{C}$.

Keywords: kaolinitisation; mineral sorting; rare earth elements; source rocks; supergene environment

1. Introduction

Kaolin refers to a clayey rock and also to a group of clay minerals consisting of kaolinite, dickite, nacrite and halloysite. Kaolinite is the most abundant kaolin mineral, whereas dickite, nacrite and halloysite are relatively rare, being commonly formed by hydrothermal alteration and occurring in sedimentary and residual deposits in association with kaolinite [1]. Kaolin is used in many industrial applications, including paper filling and coating, refractory, ceramics, fibreglass, cement, rubber, plastics, paint, catalyst and many other uses [2]. Considering its wide usage, any occurrence of kaolin is worth proper chemical, mineralogical and technological investigations [3]. A better understanding

of kaolins hinge on their environments of formation. Only a few studies have been carried out on the utilisation of kaolin in paleoenvironmental reconstruction.

Trace element and stable isotope compositions of kaolins are powerful geochemical proxies in reconstructing paleoenvironments. Trace elements (rare earth elements (REEs), large ion lithophile elements, high-field-strength elements and transition trace elements) are less mobile during sedimentary processes. This low mobility enables them to stay in the solid phase during erosion and sedimentation, thereby preserving the chemical signatures of their source rocks [4]. The concentrations of trace elements and specific ratios provide information on paleoweathering, sedimentary provenance, paleotectonics, hydraulic sorting, sediment recycling and paleo-redox conditions prevailing during the formation of kaolins [4–10].

The stable isotopic composition of kaolins can provide paleoenvironmental information on the isotopic composition of soil and meteoric waters, as well as paleotemperatures during the formation of the kaolins [11]. The stable isotope geochemistry of clay minerals has been applied in geothermometry, clay mineral genesis and diagenesis and paleoenvironments, amongst other disciplines [12–17].

In South Africa, there are a number of kaolin deposits distributed throughout the country. Most of the deposits have been studied for their geological, mineralogical and petrological properties. In Limpopo Province, the deposits have not been fully characterised, though some are being exploited for the making of bricks. This study, which is part of a mega-research on clays and clay minerals in Africa, focused on utilising trace elements and stable isotopes in two kaolins from the Lwamondo and Zebediela deposits in Limpopo Province, South Africa, to reconstruct the paleoenvironments in which they were formed.

2. Materials and Methods

2.1. Geologic Setting

The Lwamondo kaolin covers an area of about 2700 m² with an average thickness of 28 m. Half of the deposit has already been mined [18]. The Zebediela kaolin outcrop covers an area of about 3 km², having an average thickness of 130 m and an estimated volume of 390,000,000 m³. Open pit mining is on-going, with only 40% of the deposit having been mined [18]. The Lwamondo and Zebediela kaolins are classified as secondary kaolins.

The geology of the Lwamondo area is dominated by the Soutpansberg Group which is Proterozoic in age (Figure 1). The rocks of the Soutpansberg Group overlie the eastern part of the Palala shear zone and part of the Kaapvaal Craton [19]. The Soutpansberg Group represents a volcano-sedimentary succession and is subdivided into seven formations: the Tshifhefhe, Sibasa, Funduzi, Willie's Poort, Nzhelele, Stayt and Mabiligwe formations. Only four of the seven formations occur within the vicinity of the Lwamondo kaolin, namely the Tshifhefhe, Sibasa, Fundudzi and Willie's Poort formations [18]. The basal discontinuous Tshifhefhe formation is a few meters thick and made up mainly of strongly epidotised clastic sediments which include shale, greywacke and conglomerate. The Sibasa formation is mainly a volcanic succession with rare discontinuous intercalations of clastic sediments, having a maximum thickness of about 3000 m [19]. The volcanics of the Sibasa formation comprise basalts, which were subaerially extruded and minor pyroclastic rocks [20]. The basalts are amygdaloidal, massive and generally epidotised. The clastic sediments, which include quartzite, shale and minor conglomerate, can locally have a maximum thickness of 400 m [19]. The overlying Fundudzi formation is only developed in the eastern part of the Soutpansberg Group and wedges out towards the west.

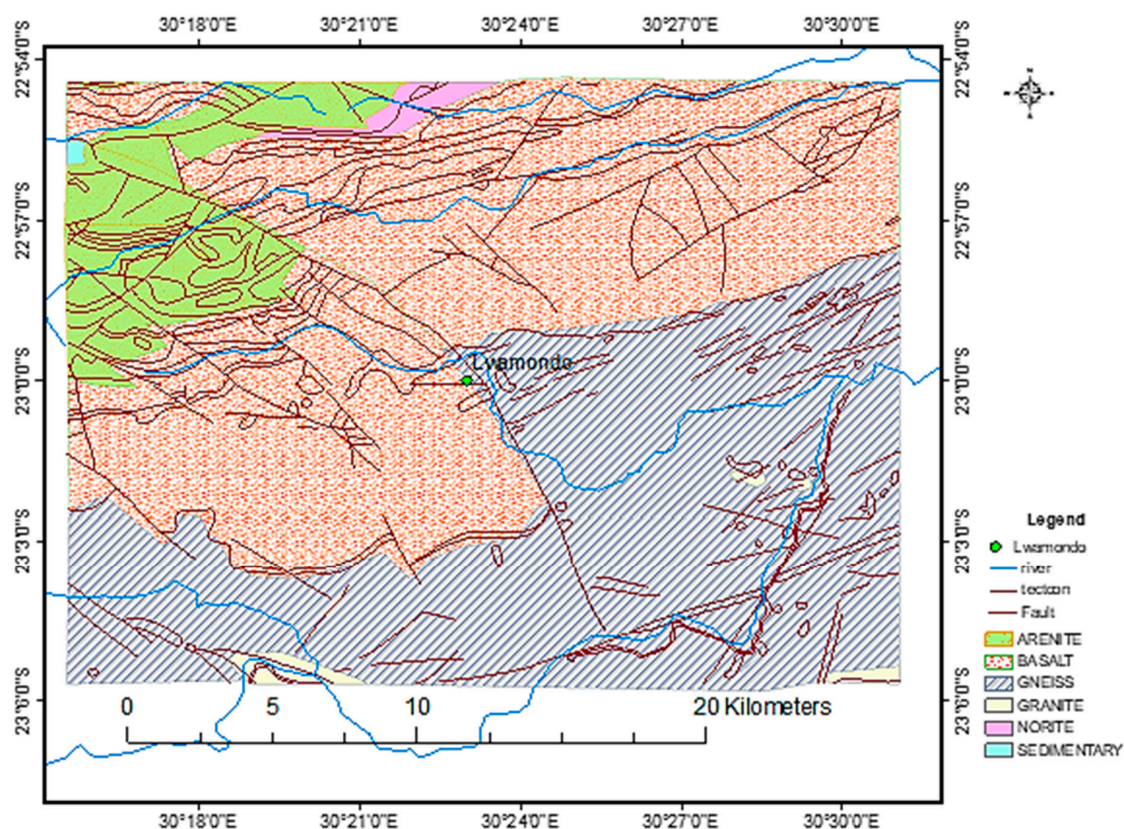


Figure 1. Geological setting of the Lwamondo kaolin occurrence. Modified from [18].

The Lwamondo kaolin was deposited within the Sibasa formation volcanic succession. The lithology of the country rocks were basalt, clastic sediments which include shale and minor conglomerates and minor pyroclastic rocks with a varicoloured kaolin (white, brownish, red, pink and yellow). The exposed outcrop at Lwamondo had an overburden with an average thickness of 2–3 m and consists of reddish brown soil. Kaolin was exposed in the lower portion of the outcrop.

The geology of Zebediela is regionally made up of rocks that belong to the Transvaal Supergroup (Figure 2). The Transvaal Supergroup is preserved in three separate basins—the Transvaal, Kanye (Botswana) and Griqualand West basins [21]—and is subdivided into four main lithostratigraphic units, namely the Protobasinal rocks, Black Reef formation, Chuniespoort Group and Pretoria Group [22]. The area is covered by surficial sediments of the Karoo Supergroup and in the northern part of the Transvaal Supergroup is controlled by ENE- and NNW-trending faults, which are common throughout the Kaapvaal Craton [18]. In the Zebediela area, the rocks belong to the Wolkberg Group followed by an unconformity-bound Black Reef formation (BRF), which in turn was overlain by the Chuniespoort Group. The Chuniespoort Group is of Proterozoic age.

Three exposed outcrops were studied and these were named as Quarry One, Quarry Three and Quarry Four. An iron-rich vein, probably an extension of the Penge banded iron formation (BIF), cut across Quarry Four. Above the iron-rich vein was a brownish to reddish kaolin layer. Kaolin of quarry one was greyish and reddish in colour. Kaolin in Quarry three was whitish with no sedimentary structure identified and within the quarry, the Zebediela kaolin was characterised by a major NNW-SE-trending fault truncated by numerous smaller veins. At Quarry Four, yellowish kaolin at the base was overlain by reddish brown, pale brown and light brown kaolin layers. These colours suggested a high iron content in the deposit.

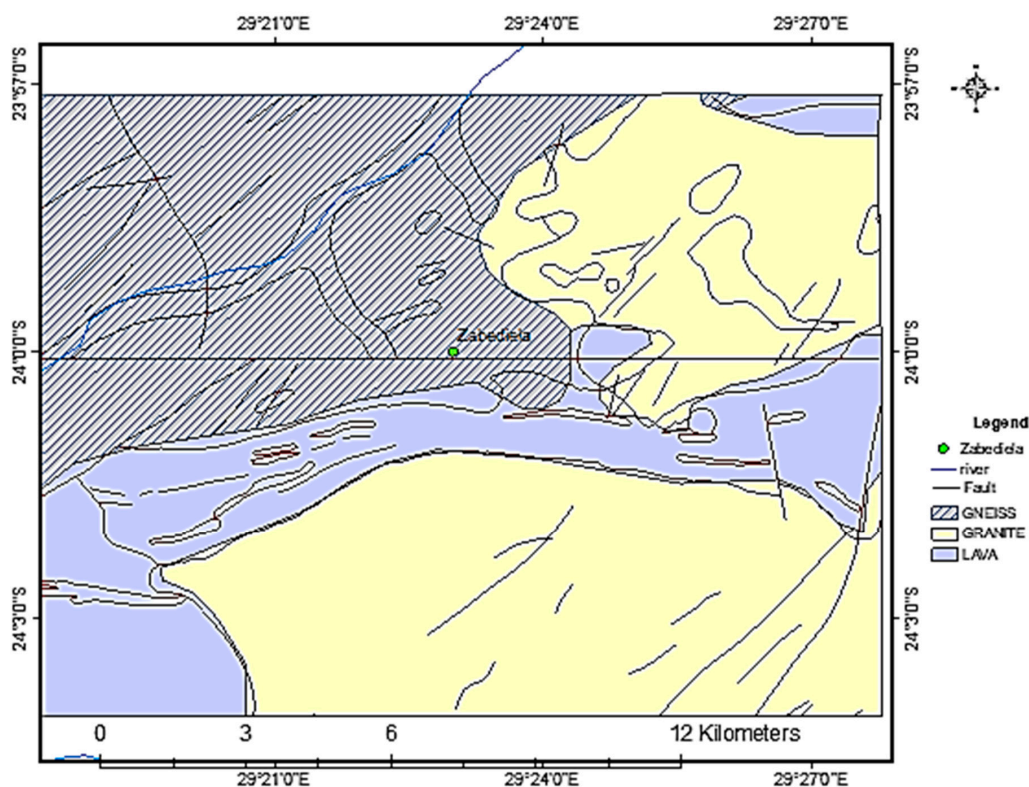


Figure 2. Geological setting of Zebediela kaolin occurrence. Modified from [18].

2.2. Sampling and Samples

Nine samples were collected from each of the two study sites. The samples were coded as LWA1–LWA9 for the Lwamondo Kaolin and ZEB1–ZEB9 for the Zebediela Kaolin. The sampling method was judgemental [3], that is, the number of samples and the sampling distance depended on the availability of exposed outcrops [23,24]. Prior to analyses, the samples were pre-treated by sieving in a 63 μm sieve, removal of organic matter, dispersion and particle size separation, based on the methods described by [25,26]. Details of particle size distribution in the studied kaolins are reported in Table 1 [27]. The analyses were performed on the <2 μm fraction of the kaolin samples, which contain more information on their environment of formation.

Table 1. Particle size distribution of the Lwamondo and Zebediela kaolins.

Sample	Sand (wt %)	Silt (wt %)	Clay (wt %)
LWA1	46	32	22
LWA2	38	40	22
LWA3	46	24	30
LWA4	20	62	18
LWA5	30	44	26
LWA6	30	34	36
LWA7	40	48	12
LWA8	22	54	24
LWA9	32	36	32
ZEB1	24	32	44
ZEB2	46	30	24
ZEB3	10	48	42
ZEB4	18	50	32
ZEB5	34	36	30
ZEB6	18	72	10
ZEB7	20	58	22
ZEB8	30	24	46
ZEB9	40	28	32

2.3. Laboratory Analyses

Kaolin samples were collected from various sites within the Lwamondo and Zebediela study areas for trace element and stable isotope analyses. Trace element analyses were carried out at the Central Analytical Facility at Stellenbosch University, South Africa, while stable isotope analyses were done at the University of Cape Town. Laser Ablation Inductively Coupled Plasma Spectrometry (LA-ICP-MS) analysis was used to determine trace element concentrations in the samples using an Agilent 7700 instrument (Agilent Technologies, Santa Clara, CA, USA). A laser was used to vaporise the surface of the solid sample, whereas the vapour and any particles were transported by the carrier gas flow to the ICP-MS. The pressed pellet method for trace element analysis (8 ± 0.05 g) of milled powder was weighed and mixed thoroughly with three drops of Mowiol wax binder. The pellet was pressed with a pill press to 15 ton pressure and was dried in an oven at 100 °C for half an hour before being analysed. Ablation was performed in He at a flow rate of 0.35 L/min and then mixed with Ar (0.9 L/min) and N (0.004 L/min) just before introduction into the IC plasma. For traces in fusions, two spots of 100 μm were ablated on each sample using a frequency of 10 Hz and energy of 3.6 mJ/cm^2 . Trace elements were quantified using Basalt, Hawaiian Volcanic Observatory (BHVO) glass [28] and BHVO powder [29] as standards, employing standard–sample bracketing. Two replicate measurements were made on each sample. The calibration standard was run after every 12 samples. The instrument’s detection limits for the analysed trace elements are shown in Table 2.

Table 2. Instrument detection limits (DL) of trace elements.

Trace Element	DL (ppm)	Trace Element	DL (ppm)
Sc	0.022	Pr	0.002
V	0.018	Nd	0.007
Cr	0.166	Sm	0.010
Co	0.008	Eu	0.002
Ni	0.144	Gd	0.007
Cu	0.020	Tb	0.001
Zn	0.130	Dy	0.004
Rb	0.008	Ho	0.001
Sr	0.003	Er	0.003
Y	0.002	Tm	0.001
Zr	0.005	Yb	0.007
Nb	0.001	Lu	0.001
Mo	0.009	Hf	0.004
Cs	0.003	Ta	0.001
Ba	0.020	Pb	0.005
La	0.001	Th	0.002
Ce	0.002	U	0.002

Oxygen isotope ratios of the $<2 \mu\text{m}$ fraction of the kaolin samples were determined after being degassed under vacuum on the silicate line at 200 °C for two hours. The samples were reacted with ClF_3 [30] in a conventional silicate line and the O_2 was converted to CO_2 using a hot platinised carbon rod. Hydrogen isotope analyses of absorbed water extracted in the manner described above were made using a variation of the closed tube Zn reduction method described by [31]. Hydrogen extraction for isotopic analysis followed the principle of [32]. After degassing at 180 °C in a vacuum to remove absorbed moisture, water was extracted from kaolin by heating in a Mo crucible with an induction furnace to >1500 °C.

3. Results

The mineral phases and major oxides of the Lwamondo and Zebediela kaolins are reported in Reference [27]. Kaolinite was the most abundant mineral phase in both kaolin deposits, with means of 68.39 wt % and 77.73 wt % in the Lwamondo and Zebediela kaolins, respectively. Other mineral phases

that were determined include quartz and smectite in major to minor quantities, clinocllore, goethite and talc in minor to trace quantities and muscovite, microcline and plagioclase in trace quantities. The most abundant oxides were SiO₂ and Al₂O₃, with respective means of 44.99 wt % and 29.82 wt % in the Lwamondo kaolin and 42.93 wt % and 31.76 wt % in the Zebediela kaolin.

3.1. Trace Elements

Trace element distribution in the clay fraction samples of the Lwamondo and Zebediela kaolins normalised to upper continental crust (UCC) values are shown in Figures 3 and 4, respectively and the results are reported in Tables 3 and 4, respectively.

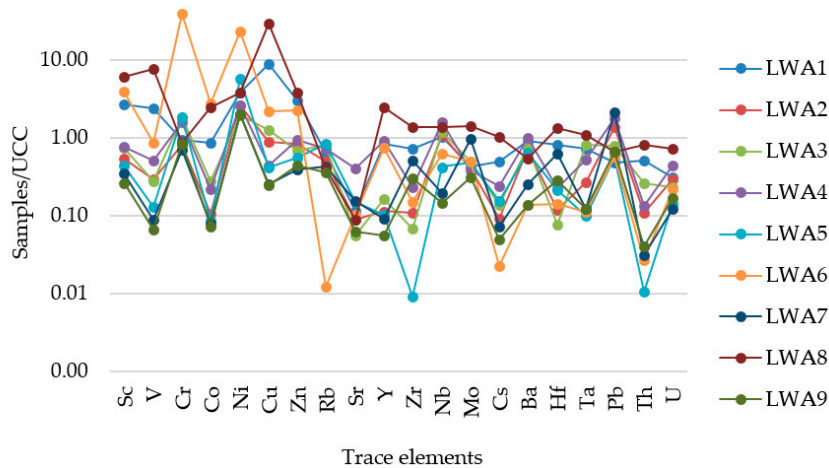


Figure 3. Upper continental crust (UCC) normalised trace element concentrations of the clay size fraction of the Lwamondo kaolin (arranged in increasing atomic number from Sc to U).

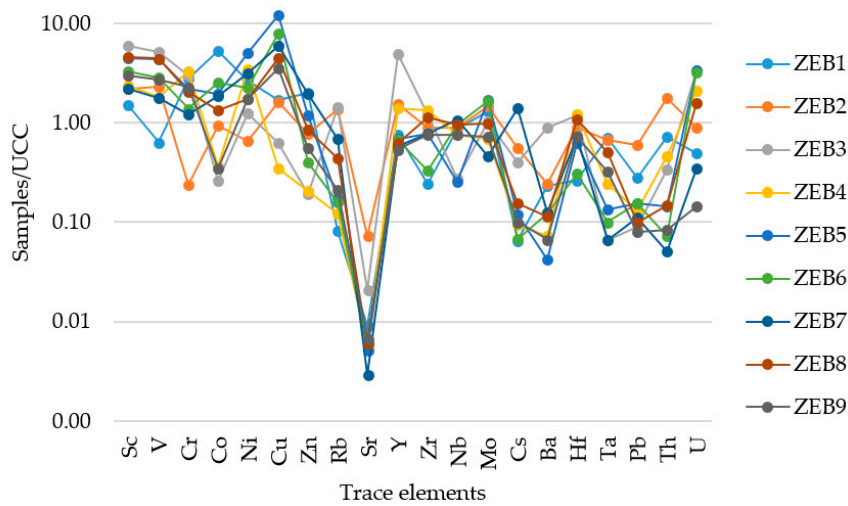


Figure 4. UCC normalised trace element concentrations of the clay size fraction of the Zebediela kaolin (arranged in increasing atomic number from Sc to U).

Table 3. Trace element composition in ppm of the clay fraction of the Lwamondo kaolin (arranged in increasing atomic number from Sc to U).

Trace Elements and Selected Ratios	LWA1	LWA2	LWA3	LWA4	LWA5	LWA6	LWA7	LWA8	LWA9	UCC ¹
Sc	37.2	7.6	10.6	10.6	6.1	55.0	4.9	85.5	3.7	14.0
V	230.4	28.1	26.6	49.6	12.7	82.7	8.6	738.0	6.5	97.0
Cr	85.6	75.0	171.6	145.5	168.9	3604.0	64.2	79.6	76.1	92.0
Co	15.1	1.8	4.9	3.8	1.5	48.6	1.4	42.7	1.3	17.3
Ni	178.8	123.3	93.0	122.0	269.0	1082.5	94.6	178.6	94.0	47.0
Cu	247.0	24.6	35.4.0	12.4	11.8	62.1	7.1	828.0	6.9	28.0
Zn	200.6	55.9	46	63.1	37.2	151.7	26.7	253.0	29.8	67.0
Rb	53.7	41.9	68.7	61.6	70.5	1.0	35.9	33.5	30.3	84.0
Sr	37.2	28.3	18.0	128.7	48.0	33.2	49.0	28.5	20.0	320.0
Y	17.4	2.4	3.4	19.4	2.2	15.5	1.9	52.4	1.2	21.0
Zr	140.1	21.1	13.3	45.0	1.8	29.0	99.5	266.4	59.0	193.0
Nb	12.5	13.0	14.2	18.9	5.1	7.5	2.4	16.3	1.7	12.0
Mo	0.5	0.4	0.5	0.4	0.5	0.6	1.1	1.6	0.3	1.1
Cs	2.4	0.5	0.7	1.2	0.8	0.1	0.4	5.0	0.2	4.9
Ba	562.5	450.0	484.5	626.0	404.5	86.6	157.0	340.5	85.8	624.0
Hf	4.3	0.6	0.4	1.2	1.2	0.8	3.4	7.1	1.5	5.3
Ta	0.7	0.2	0.7	0.5	0.1	0.1	0.1	1.0	0.1	0.9
Pb	8.3	23.4	13.5	30.1	9.4	9.8	35.8	11.2	11.4	17
Th	5.4	1.1	2.8	1.4	0.1	0.3	0.3	8.5	0.4	10.5
U	0.8	0.8	0.6	1.2	0.4	0.6	0.3	2.0	0.5	2.7
U/Th	0.2	0.7	0.2	0.8	3.5	2.1	1.0	0.2	1.1	
Ni/Co	11.9	67.4	19.2	32.1	181.8	22.3	70.1	4.2	74.0	
V/Cr	2.7	0.4	0.2	0.3	0.1	0.0	0.1	9.3	0.1	

¹ Upper continental crust (UCC) values from [33].

Table 4. Trace element composition in ppm of the clay size fraction of the Zebediela kaolin (arranged in increasing atomic number from Sc to U).

Trace Elements and Selected Ratios	ZEB1	ZEB2	ZEB3	ZEB4	ZEB5	ZEB6	ZEB7	ZEB8	ZEB9	UCC ¹
Sc	20.9	30.6	83.6	33.3	62.3	46.4	30.6	63.7	41.8	14
V	61.5	223.0	504.0	174.2	425.9	273.6	172.6	428.0	263.6	97
Cr	253.6	21.7	272.8	299.0	203.9	127.2	110.9	188.1	209.4	92
Co	92.3	16.1	4.5	6.2	33.8	43.8	32.4	22.9	6.0	17.3
Ni	124.8	30.8	57.9	163.3	237.9	106.8	147.2	81.9	82.2	47
Cu	47.2	45.1	17.7	9.8	335.5	219.2	165.0	125.3	98.5	28
Zn	133.4	51.7	12.9	13.9	80.2	26.8	130.8	57.3	37.0	67
Rb	6.8	115.2	120.1	10.3	14.6	13.3	57.3	37.2	17.8	84
Sr	2.9	23.5	6.6	1.8	1.7	2.0	0.9	2.0	2.2	320
Y	15.9	32.3	103.2	29.5	14.5	14.1	12.2	13.2	11.3	21
Zr	47.4	172.2	232.9	257.0	150.2	63.8	148.4	217.6	147.6	193
Nb	10.5	10.8	3.3	9.1	3.08	11.6	12.8	11.4	9.2	12
Mo	1.4	1.6	1.1	0.8	1.9	1.8	0.5	1.1	0.8	1.1
Cs	0.3	2.7	2.0	0.5	0.6	0.3	6.8	0.8	0.5	4.9
Ba	143.6	150.7	554.0	45.2	26.6	75.8	78.3	70.4	41.7	624
Hf	1.4	4.7	6.3	6.5	3.3	1.6	3.8	5.7	3.8	5.3
Ta	0.6	0.6	0.1	0.2	0.11	0.1	0.1	0.5	0.3	0.9
Pb	4.7	10.1	1.5	2.2	2.6	2.7	1.9	1.7	1.4	17
Th	7.6	18.7	3.5	4.8	1.5	0.8	0.5	1.6	0.9	10.5
U	1.3	2.4	9.0	5.7	9.0	8.8	0.9	4.3	0.4	2.7
U/Th	0.2	0.1	2.6	1.18	6.0	11.5	1.8	2.8	0.5	
Ni/Co	1.4	1.9	12.9	26.21	7.0	2.4	4.5	3.6	13.8	
V/Cr	0.2	10.3	1.9	0.58	2.1	2.2	1.6	2.3	1.3	

¹ UCC values from [33].

Large ion lithophile elements (Rb, Ba, Sr, Th, U): Compared to the UCC, large ion lithophile elements are generally depleted in the Lwamondo kaolins (Figure 3). Rubidium is most depleted in LWA6, whereas Th is more depleted in LWA5. Sample LWA4 has almost the same concentration of Ba as the UCC and this sample is also the least depleted in Sr. The UCC normalised concentrations of large ion lithophile elements in the Zebediela kaolins show that Sr is the most depleted trace element and is depleted in all the samples (Figure 4). Barium is slightly depleted in all Zebediela samples. Rubidium is only enriched in ZEB2 and ZEB3, Th is only enriched in ZEB4 and U is depleted in samples ZEB2, ZEB1, ZEB5 and ZEB9.

High field strength elements (Zr, Hf, Y, Nb): Compared to the UCC, sample LWA8 is the only sample enriched in all high-field-strength elements (Figure 3). Niobium is depleted in samples LWA5, LWA6, LWA7 and LWA9, whereas it is slightly enriched in samples LWA1, LWA2, LWA3, LWA4 and LWA8 compared to the UCC. Zirconium is most depleted in LWA5, while Hf is more depleted in LWA3. In the Zebediela kaolins, UCC normalised high-field-strength elements are generally slightly depleted, except in ZEB2 and ZEB4, which are similar to the UCC (Figure 4).

Transition trace elements (V, Co, Cu, Ni and Sc): Nickel is enriched in the Lwamondo kaolins compared to the UCC (Figure 3). Sc is enriched in samples LWA1, LWA6 and LWA8 and depleted in samples LWA2, LWA3, LWA4, LWA5, LWA7 and LWA9. Vanadium is only enriched in LWA1 and LWA8, Co is enriched in LWA1 and LWA6 and Cu is enriched in samples LWA1, LWA3, LWA6 and LWA8 (Figure 3). The UCC normalised transition trace elements are generally enriched in the Zebediela kaolins (Figure 4). Scandium is enriched in all Zebediela samples; so is V, except in ZEB1. Co and Cu are slightly depleted in ZEB3 and ZEB4. Ni is only depleted in ZEB2.

3.2. Rare Earth Elements (REEs)

Results of UCC normalised REEs of the Lwamondo and Zebediela kaolins are plotted in Figures 5 and 6 and shown in Tables 5 and 6. There is a slight enrichment of heavy rare earth elements (HREEs) compared to light rare earth elements (LREEs) in these kaolins (Figures 5 and 6).

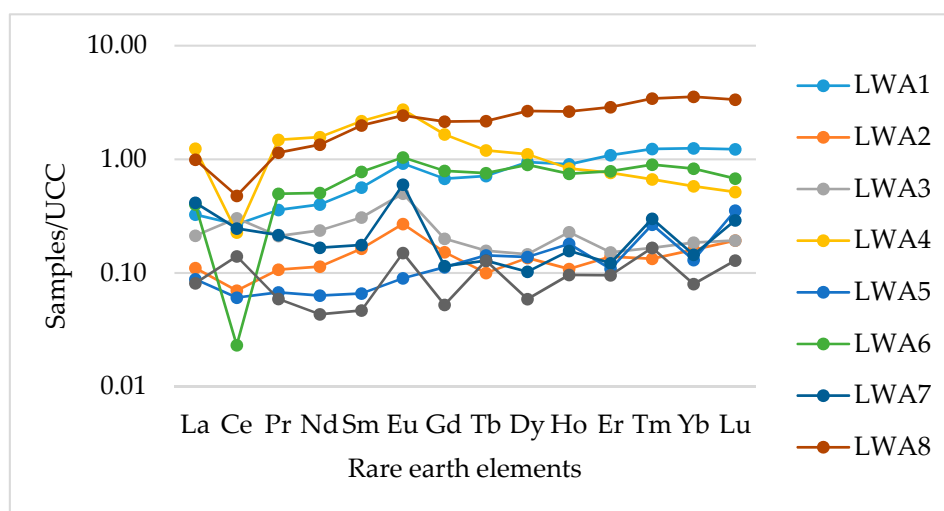


Figure 5. Rare earth element plot of the clay size fraction of the Lwamondo kaolin samples compared to the UCC.

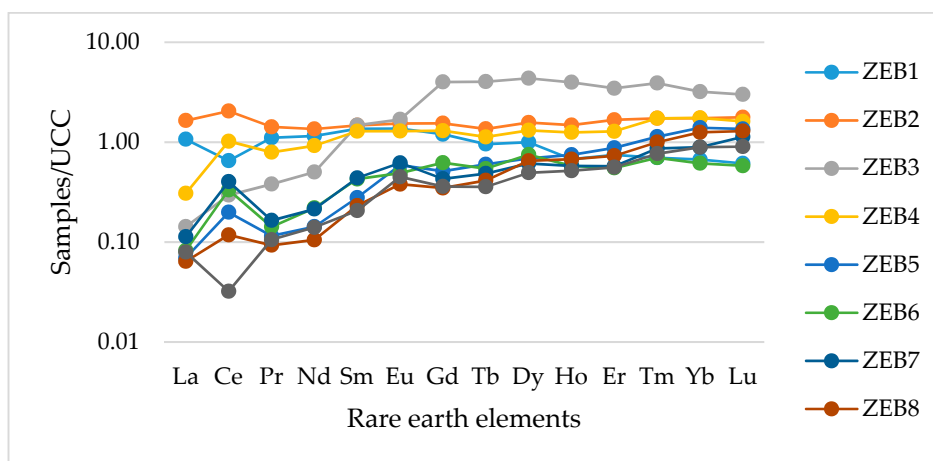


Figure 6. Rare earth element plot of the clay size fraction of the Zebediela kaolin samples compared to the UCC.

Table 5. Rare earth element composition in ppm of the clay fraction of the Lwamondo kaolin.

Rare Earth Elements	LWA1	LWA2	LWA3	LWA4	LWA5	LWA6	LWA7	LWA8	LWA9	UCC ¹
La	10.1	3.4	6.6	38.6	2.7	12.4	12.9	30.8	2.5	31
Ce	16.9	4.4	19.1	14.3	3.8	1.5	15.5	30.3	8.8	63
Pr	2.6	0.8	1.5	10.6	0.5	3.5	1.5	8.4	0.4	7.1
Nd	10.8	3.1	6.4	42.4	1.7	13.7	4.5	36.4	1.2	27
Sm	2.7	0.8	1.5	10.2	0.3	3.7	0.8	9.4	0.2	4.7
Eu	0.9	0.3	0.5	2.7	0.1	1.0	0.6	2.4	0.2	1
Gd	2.7	0.6	0.8	6.6	0.5	3.2	0.5	8.6	0.2	4
Tb	0.5	0.1	0.1	0.8	0.1	0.5	0.1	1.5	0.1	0.7
Dy	3.7	0.5	0.6	4.3	0.5	3.5	0.4	10.4	0.2	3.9
Ho	0.8	0.1	0.2	0.7	0.2	0.6	0.1	2.2	0.1	83
Er	2.5	0.3	0.4	1.8	0.3	1.8	0.3	6.6	0.2	2.3
Tm	0.4	0	0.1	0.2	0.1	0.3	0.1	1.0	0.1	0.3
Yb	2.5	0.3	0.4	1.2	0.3	1.7	0.3	7.1	0.2	2
Lu	0.4	0.1	0.1	0.2	0.1	0.2	0.1	1.0	0	0.3
ΣLREE	46.7	13.4	36.4	125.4	9.6	39	36.3	126.3	13.5	137.8
ΣHREE	10.8	1.4	1.8	9.2	1.6	8.6	1.4	29.8	0.9	92.5
ΣREE	57.5	14.8	38.3	134.6	11.2	47.6	37.8	156.1	14.4	230.3

¹ UCC values from [33].

Table 6. Rare earth element composition in ppm of the clay size fraction of the Zebediela kaolin.

Rare Earth Elements	ZEB1	ZEB2	ZEB3	ZEB4	ZEB5	ZEB6	ZEB7	ZEB8	ZEB9	UCC ¹
La	33.1	51.0	4.4	9.6	2.2	2.6	3.5	2	2.5	31
Ce	41.1	129	18.6	64.3	12.5	21	25.4	7.4	2	63
Pr	7.9	10.1	2.7	5.6	0.8	1	1.2	0.7	0.8	7.1
Nd	31.1	36.6	13.6	24.9	3.9	5.9	5.8	2.8	3.8	27
Sm	6.4	6.9	7	6.1	1.3	2.0	2.1	1.1	1	4.7
Eu	1.4	1.5	1.7	1.3	0.6	0.5	0.6	0.4	0.5	1
Gd	4.8	6.2	16	5.2	2.1	2.5	1.7	1.4	1.4	4
Tb	0.7	1	2.8	0.8	0.4	0.4	0.3	0.3	0.3	0.7
Dy	3.9	6.1	17	5.1	2.7	2.9	2.4	2.5	1.9	3.9
Ho	0.6	1.2	3.3	1	0.6	0.5	0.5	0.6	0.4	0.8
Er	1.7	3.9	8	3	2	1.3	1.3	1.7	1.3	2.3
Tm	0.2	0.5	1.2	0.5	0.3	0.2	0.3	0.3	0.2	0.3
Yb	1.3	3.5	6.4	3.5	2.8	1.2	1.8	2.5	1.8	2
Lu	0.2	0.6	0.9	0.5	0.4	0.2	0.4	0.4	0.3	0.3
ΣLREE	125.8	241.3	64	117	23.4	35.5	40.3	15.8	12	137.8
ΣHREE	8.6	16.8	39.6	14.4	9.2	6.7	7	8.3	6.2	10.3
ΣREE	134.4	258.1	103.6	131.4	32.6	42.2	47.3	24.1	18.2	148.1

¹ UCC values from [33].

3.3. Hydrogen and Oxygen Isotopes

The stable isotope values of kaolinite from Lwamondo vary from 17.4‰ to 19.2‰ $\delta^{18}\text{O}$, with a mean of 18.6‰ and from -54‰ to 84‰ δD , with a mean of -65.3‰ (Table 7). The mean water content is 10.63%. The Zebediela kaolinite has the following stable isotope values: $\delta^{18}\text{O}$ values range from 16.7‰ to 17.7‰, with a mean value of 16.7‰ and the δD values range between -68‰ and -61‰ , with a mean value of -65.3‰ (Table 7). The mean water content in the Zebediela kaolins is 10.86%. The binary plot of $\delta^{18}\text{O}$ and δD values shows that most samples fall in the supergene field (Figure 7).

Table 7. H_2O yields and $\delta^{18}\text{O}$ and δD values of the Lwamondo and Zebediela kaolins.

Sample	$\delta^{18}\text{O}$ (‰)	δD (‰)	H_2O (%)
LWA1	17.4	-84	8.48
LWA2	19.2	-58	12.05
LWA9	19.1	-54	11.37
Mean	18.6	-65	10.63
ZEB2	16.7	-68	10.16
ZEB4	17.7	-61	11.67
ZEB8	15.6	-63	10.74
Mean	16.7	-64	10.86

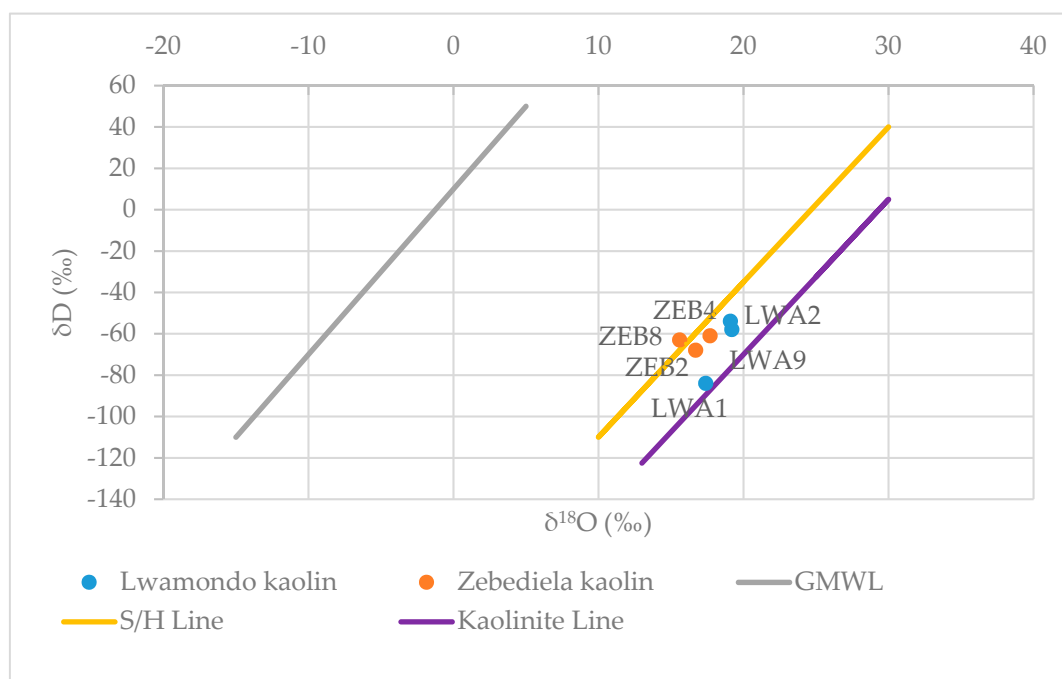


Figure 7. $\delta^{18}\text{O}$ versus δD plot of clay fractions of the Lwamondo and Zebediela kaolins. The global meteoric water line (GMWL), the supergene–hypogene line (S/H line) and the kaolinite line are plotted for reference.

4. Discussion

The distribution of trace elements in clays is influenced by sedimentary processes (such as weathering, sorting and sedimentary recycling) and sedimentary provenance, such as the nature of parent rocks [34,35]. The stable isotopic composition of kaolins contains information about temperatures.

4.1. Paleoweathering

The higher concentration of Cr and V in the studied kaolin may be related to their low mobility during the kaolinitisation process [36]. The Lwamondo and Zebediela kaolins were also enriched in Ni, except sample ZEB2 which is related to it being easily mobilized during weathering. Barium and Sr were depleted in all samples, indicating that they were easily mobilized during weathering and removed from the environment [37,38]. During kaolinitisation, Sc was slightly concentrated in the kaolin deposit and was enriched in all samples except in samples LWA1, LWA6 and LWA8.

The HREEs are more enriched than LREEs in the weathered and sub-weathered zones [39]. The REE patterns show more enrichment in HREEs than LREEs in all samples, with slight positive Eu anomaly due to the presence of plagioclase in the kaolin samples. The REE pattern and the content of other trace elements show evidence of weathering related to kaolinitisation in the Lwamondo and Zebediela kaolins.

4.2. Sedimentary Provenance and Tectonic Setting

The concentrations of some trace elements, such as Th, Sc, Cr, La, Ni and Co and their ratios varied in different source rock composition (silicic and basic). Therefore, they are widely used for provenance studies, as they are transported almost exclusively in the terrigenous component of sediment, thereby reflecting the chemistry of their source rocks [4]. Felsic rocks are richer in Th and La, whereas mafic rocks are richer in Co, Sc, Ni and Cr [9]. Hence, these elements and their ratios (La/Sc, Th/Sc, Th/Co and Cr/Th) could be used to infer the sedimentary provenance or source rock composition [7,8]. Figure 8 shows a basic source of the Zebediela kaolins and an intermediate-to-silicic source of the Lwamondo kaolins, whereas Figure 9 shows a felsic source of these kaolins.

High concentrations of Cr (>150 ppm) and Ni (>100 ppm), low Cr/Ni ratios (<1.5) and a high correlation coefficient between Cr and Ni (>0.90) are indicative of an ultramafic rock source, whereas a Cr/Ni ratio >2.0 indicates mafic-volcanic detritus [40]. Concentrations of Cr and Ni in the Lwamondo and Zebediela kaolins were very varied, even among samples in the same location. In general, Ni concentrations were greater than 100 ppm and Cr concentrations were greater than 150 ppm. The correlation coefficient between Cr and Ni was 0.98 and 0.33 in the Lwamondo and Zebediela kaolins, respectively. This shows that although an ultramafic or mafic source could be inferred for the Lwamondo kaolin, such sources cannot be inferred for the Zebediela kaolin.

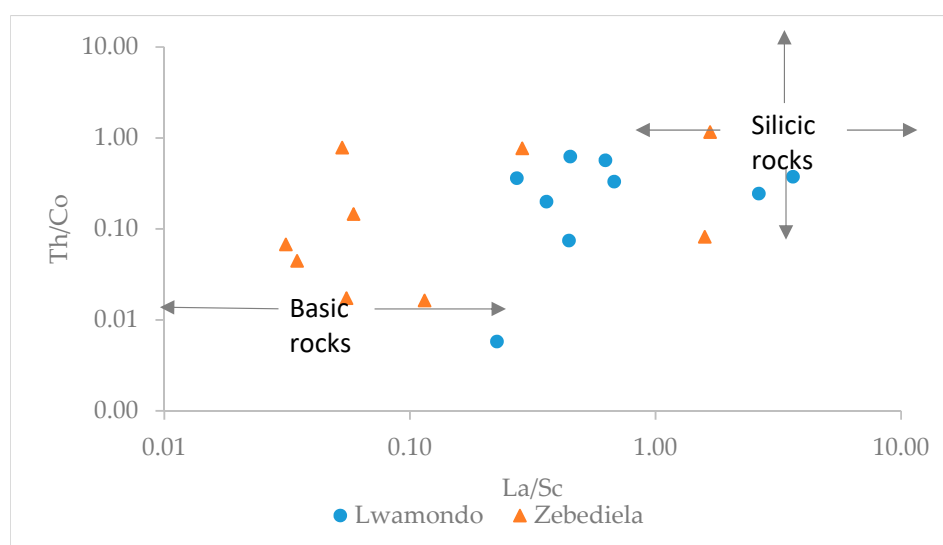


Figure 8. Th/Co vs. La/Sc showing the source rocks of the Lwamondo and Zebediela kaolins.

The Lwamondo kaolin deposit is located in the Sibasa formation and there are basalts which rest on the basements of the Hoot Plaats gneiss and granite. The observed kaolin deposit was ferruginous

and whitish. The geology of the area suggests that kaolin may have been formed from basalt and clastic sediments. The surrounding country rocks are believed to have provided the primary minerals for kaolinitisation.

The field observation from the Zebediela kaolin is similar to the one reported by [13,41] of the Kgwakgwe kaolins in Botswana. The thickness of the beds in the Zebediela kaolin deposit showed different colours (pinkish, yellowing and reddish) and layerings, which depict beds of a sedimentary nature. The kaolin deposit is penetrated by reddish veins which probably mark groundwater passages. Surrounding country rocks are arkose mudstone and shale which are considered to have provided primary minerals for kaolinitisation.

The Th/U ratio can also give an indication of the source of kaolins [5]. Low Th/U ratios (<3.5) are usually found in mantle-derived rocks, though sediments from active margin tectonic settings with major components of young undifferentiated crust could also have Th/U ratios <3.5 [5]. Due to the low concentrations of U and Th in the Lwamondo and Zebediela kaolins (Figure 10), it is suggested that these kaolins are derived from an active margin tectonic setting.

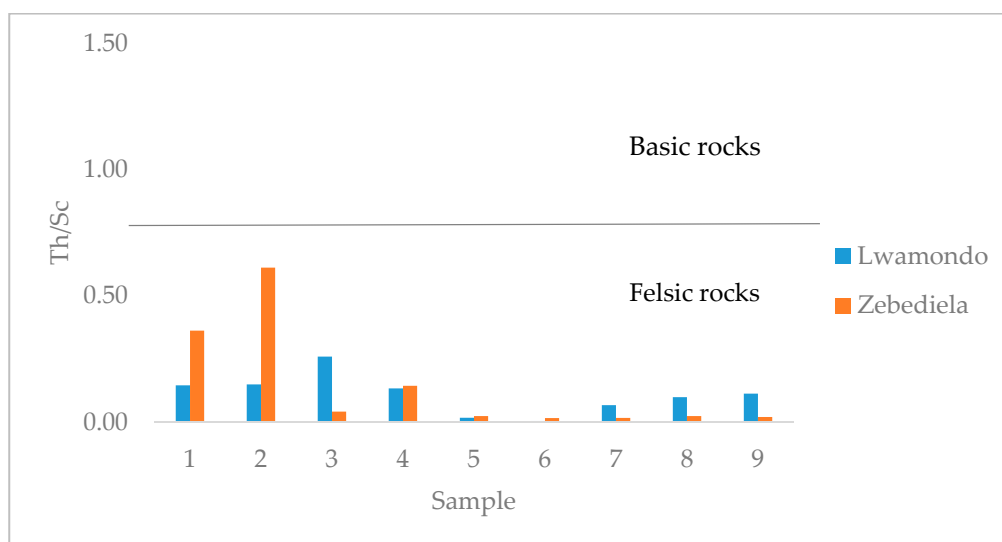


Figure 9. Plot of Th/Sc of the Lwamondo and Zebediela kaolins, showing a silicic source.

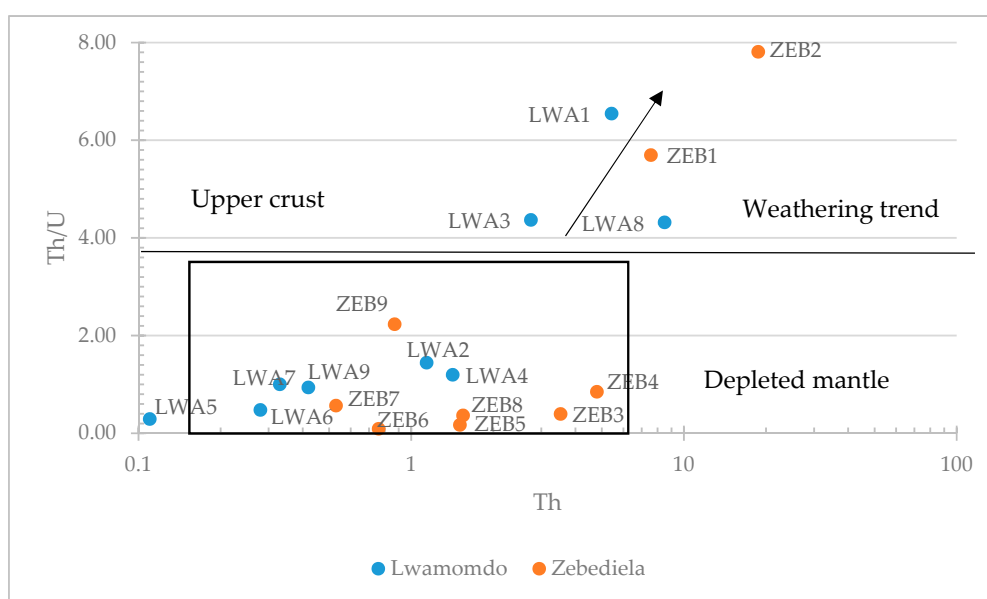


Figure 10. Plot of Th/U vs. Th for the Lwamondo and Zebediela kaolins, showing a mantle source.

4.3. Hydraulic Sorting and Sediment Recycling

The Th/Sc versus Zr/Sc bivariate plot can be used to illustrate hydraulic sorting and sedimentary recycling [5]. Whereas Th is incompatible in igneous systems, Sc is compatible in igneous systems [14]. Therefore, the Th/Sc ratio is a good proxy for igneous chemical differentiation processes. Unlike Zr, which is strongly enriched in zircon, Sc is not enriched but generally preserves a signature of the provenance. The Zr/Sc ratio is a useful index for zircon enrichment [5]. Trend 1 on this plot (Figure 11) shows the normal igneous differentiation trend, which does not involve zircon enrichment. An enrichment of zircon occurs during sedimentary sorting or recycling (Trend 2) [10]. Figure 11 shows that the Lwamondo and Zebediela kaolins are generally around Trend 1, suggesting minimum mineral sorting [9].

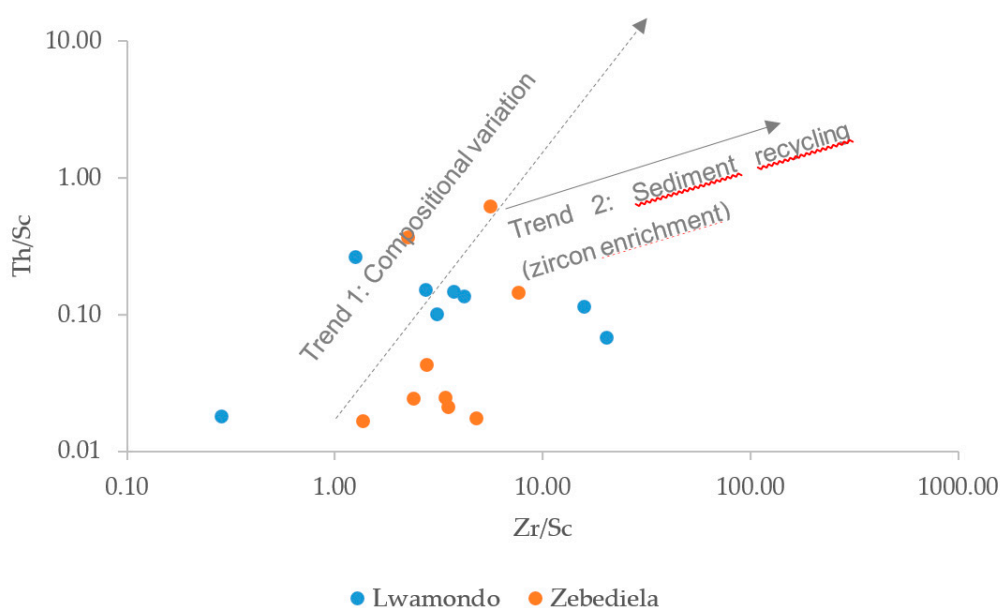


Figure 11. Th/Sc vs. Zr/Sc plot showing the normal trend for compositional variation in the Lwamondo and Zebediela kaolins.

4.4. Paleo-Redox Conditions

U/Th ratios <1.25 suggest an oxic condition of deposition, whereas values >1.25 indicate suboxic and anoxic conditions [6]. Most of the Lwamondo kaolin showed low U/Th (0.15–3.45, average of 1.09), which indicates that the kaolin was deposited in an oxic environment; by contrast, the Zebediela kaolin displays high U/Th ratios (0.18–11.5, average of 2.95), which indicates that the kaolin was deposited under suboxic/anoxic conditions. A V/Cr ratio <2 indicates oxic, 2.0–4.25 indicates dysoxic and >4.25 indicates suboxic to anoxic conditions [6]. The V/Cr ratios of the Lwamondo kaolin samples varied from 0.02–9.27, with an average of 1.40, indicating an oxic condition (Figure 12), whereas the V/Cr ratios of the Zebediela kaolin varied from 0.24–10.28, with an average of 2.48, indicating an oxic condition (Figure 12).

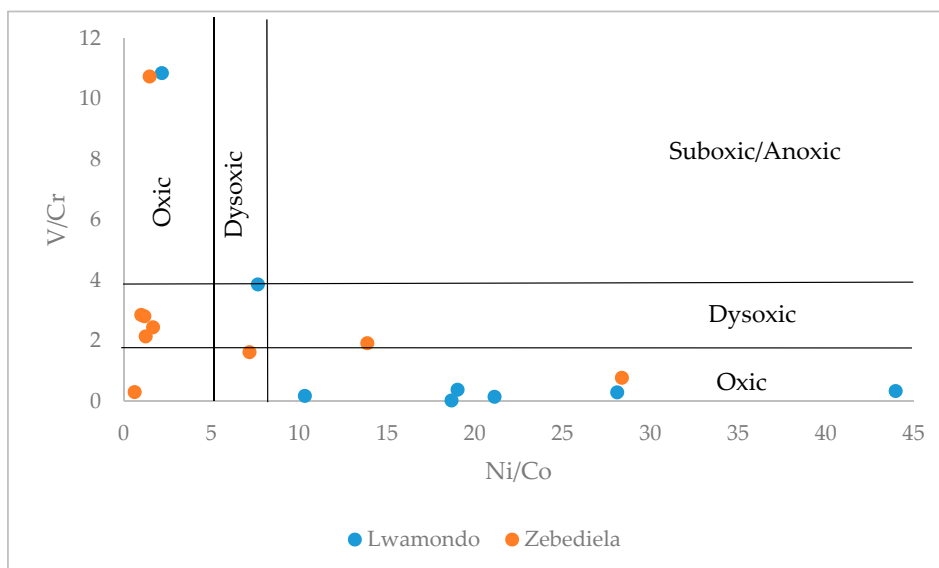


Figure 12. Cross plots of V/Cr vs. Ni/Co used as paleo-redox proxies.

4.5. Paleotemperatures

Kaolin can be formed through interactions with modern local meteoric water. The isotopic composition of kaolinite was determined using the mean isotopic composition of modern meteoric water and equilibrium fractionation factors between kaolinite and water (Equations (1) and (2)) by [42]:

$$\alpha_{K-W}^O = \frac{\delta^{18}O_K + 1000}{\delta^{18}O_W + 1000} \tag{1}$$

$$\alpha_{K-W}^D = \frac{\delta D_K + 1000}{\delta D_W + 1000} \tag{2}$$

where α_{K-W}^O and α_{K-W}^D are equilibrium fraction factors between kaolinite and water (meteoric water) with respect to oxygen and hydrogen [43].

The isotopic composition of kaolinite was determined using the modern mean annual temperature based on Equations (3) and (4):

$$\text{Hydrogen : } 1000 \ln \alpha_{kaolinite-water} = -2.2 \times 10^6 x T^{-2} - 7.7 \tag{3}$$

$$\text{Oxygen : } 1000 \ln \alpha_{kaolinite-water} = 2.76 \times 10^6 x T^{-2} - 6.75 \tag{4}$$

where T is the temperature ($^{\circ}K$) and $\alpha_{kaolinite-water}$ is equilibrium isotopic fractionation factors between kaolinite and water.

The stable isotope composition of kaolins, as well as other clay minerals, is a function of the isotopic composition of the water from which they were formed. The equilibrium isotopic fractionation factors between kaolinite and water were developed by [44] and [12]. These fractionation factors are a function of the temperature of kaolinitisation; therefore, the isotopic composition of kaolinite can provide information about its genesis [15].

The temperature of kaolinitisation (T) of the studied kaolins were calculated using Equation (5) [16] and is presented in Table 8. The Lwamondo kaolin deposit had a mean temperature of 26.9 ± 3.6 $^{\circ}C$ whereas the Zebediela kaolin had a mean temperature of 36.6 ± 4.2 $^{\circ}C$. Kaolinite in equilibrium with the global meteoric water line, kaolinitisation temperatures in the Lwamondo kaolins (26.9 $^{\circ}C$), whereas the Zebediela kaolins kaolinitisation temperature was 36.6 $^{\circ}C$. The Makoro and Kgwakgwe kaolins formed at around 40 $^{\circ}C$ [39]. Therefore, based on their stable isotopic compositions, the Lwamondo and Zebediela kaolins were formed at low temperatures (<40 $^{\circ}C$), thus ruling out any

possible hydrothermal process. The position of sample ZEB8 in the hypogene field could be interpreted as reflecting formation in isotopic equilibrium with its parental fluid without subsequent isotopic exchange with meteoric water [44].

$$3.04 \times 10^6 T^{-2} = \delta O_K - 0.125 \delta D_K + 7.04 \tag{5}$$

Table 8. Calculated temperatures of kaolinitisation (*T*) of the analysed samples.

Samples	$\delta^{18}O$ (‰)	Δd (‰)	<i>T</i> (°C)
LWA1	17.4	−84	21.8
LWA2	19.2	−58	28.1
LWA9	19.1	−54	30.9
MEAN	18.6	−65	26.9 ± 3.6
ZEB2	16.7	−68	33.9
ZEB4	17.7	−61	33.3
ZEB8	15.6	−63	42.5
MEAN	16.7	−64	36.6 ± 4.2

The mean temperature of kaolinitisation was determined using the global meteoric water line (GMWL). This was used to determine the mean stable isotopic composition of the meteoric water in equilibrium with the Lwamondo and Zebediela kaolins during their formation using Equations (3) and (4). The calculated mean isotopic composition of meteoric water is shown in Table 9. Using the GMWL equation, the mean calculated isotopic composition of the meteoric water in equilibrium with the Lwamondo kaolins is −5.3‰ and −33.2‰ for $\delta^{18}O_W$ and δD_W , respectively, whereas the mean calculated isotopic composition of meteoric water in equilibrium with the Zebediela kaolin is −5.4‰ and −33.4‰ for $\delta^{18}O_W$ and δD_W , respectively (Table 9 and Figure 13). The equilibrium fractionation factor of deuterium (D) between kaolinite and water ($\alpha_{K-W D}$) of the Lwamondo and Zebediela kaolins calculated using the GMWL was 0.97 and 0.97, whereas the equilibrium fractionation factor of ^{18}O between kaolinite and water of the Lwamondo and Zebediela kaolins was 1.024 and 1.022 (Table 9).

Table 9. Mean isotopic composition of meteoric water and kaolinite–water fractionation factors.

Samples	$\delta^{18}O_K$ (‰)	δD_K (‰)	<i>T</i> (°K)	$\delta^{18}O_W$ (‰)	δD_W (‰)	$\alpha_{K-W}^{18}O$	$\alpha_{K-W D}$
Lwamondo	18.6	−65	300.1	−5.3	−33.2	1.024	0.97
Zebediela	16.7	−64	309.7	−5.4	−33.4	1.022	0.97

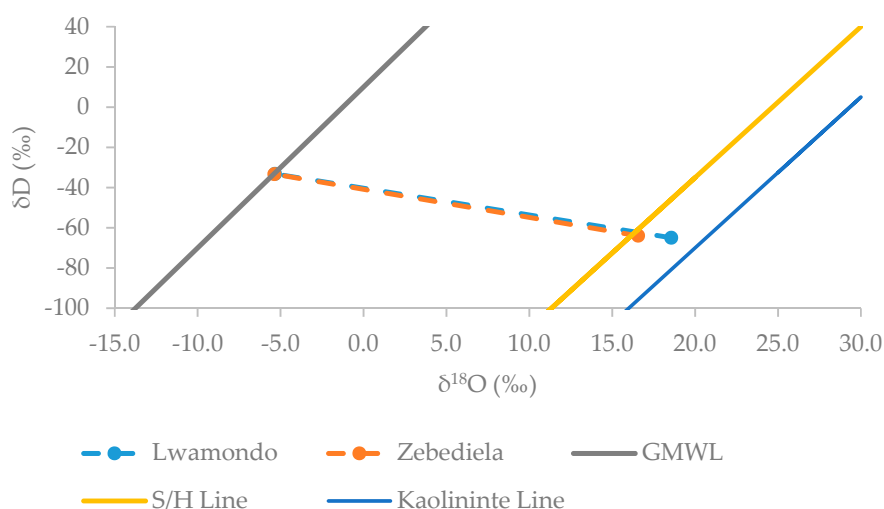


Figure 13. $\delta^{18}O$ vs. δD diagram for <2 μm fraction of the Lwamondo and Zebediela kaolins. The GMWL, S/H Line and kaolinite lines are given as reference.

The isotopic compositions of the Lwamondo and Zebediela kaolins indicate that they are of weathering origin and formed in a supergene environment. Kaolins of weathering origin generally have higher $\delta^{18}\text{O}$ (from 17‰ to 23‰) and δD (from -80‰ to 40‰) values. This is supported by data of the following kaolins of weathering origin: Nuevo Montecastelo kaolins in Spain [43], Variscan kaolins in Spain [16], Burela kaolin in Spain [45], Lastarria kaolin in Chile [17] and La Espingarda kaolin in Patagonia [46].

The major controlling factor in the clay mineral assemblages is the water composition in the environment of deposition [47]. The 2:1 layer silicates are dissolved by fresh water, which enhances kaolinite formation [48], whereas sea water preserves and promotes the genesis of mica, chlorite and smectite [49]. The mineralogy of the studied Lwamondo and Zebediela kaolins being dominated by kaolinite is indicative of relatively uniform chemistry from the processes of weathering, transportation, deposition and their reworkings.

5. Conclusions

Trace element and stable isotope compositions of the Lwamondo and Zebediela kaolins were studied in order to determine the paleoenvironmental conditions underpinning their formation. The REE pattern and the content of various trace elements showed evidence of ongoing kaolinitisation in the Lwamondo and Zebediela kaolins, with minimum mineral sorting. The host rocks for the studied kaolins varied from basic to intermediate for the Zebediela kaolin deposit and from intermediate to felsic for the Lwamondo deposit. The U and Th contents of the Lwamondo and Zebediela kaolins suggest that these kaolins were derived from an active margin tectonic setting. The Lwamondo kaolin was deposited in an oxic environment, whereas the Zebediela kaolin was deposited under suboxic/anoxic conditions. The $\delta^{18}\text{O}$ and δD values of the kaolinite from the Lwamondo and Zebediela kaolin deposits suggest that they were formed during weathering consistent with supergene origin. The mean $\delta^{18}\text{O}$ and δD isotopic values of the studied samples indicate that the kaolin formation was in equilibrium with meteoric water at near-surface temperature. The temperature of formation of the Lwamondo and Zebediela kaolins based on their stable isotope values is indicative of the low temperature of kaolinitisation, ruling out any possible hydrothermal process.

Author Contributions: Conceptualization, A.R. and G.-I.E.; Formal analysis, A.R.; Funding acquisition, A.R. and G.-I.E.; Investigation, A.R.; Project administration, G.-I.E.; Supervision, G.-I.E., J.O. (John Odiyo), J.O. (Jason Ogola) and N.B.; Validation, G.-I.E.; Writing—original draft, A.R.; Writing—review and editing, G.-I.E., J.O. (John Odiyo), J.O. (Jason Ogola) and N.B.

Funding: This research was funded by the National Research Foundation (South Africa), grant number UID 95472 and the University of Venda's Research and Publications Committee grant number RI/14/RI/01.

Acknowledgments: The authors are grateful to the management of Lwamondo Vhavenda Bricks and Zebediela Bricks for allowing the field component of the study to take place in their premises.

Conflicts of Interest: The authors declare no conflict of interest. The funders had no role in the design of the study, in the collection, analyses or interpretation of data, in the writing of the manuscript or in the decision to publish the results.

References

1. Murray, H.H. Applied Clay Mineralogy. Occurrences, processing and application of kaolins, bentonites, palygorskite-sepiolite and common clays. In *Developments in Clay Science*; Elsevier: Amsterdam, The Netherlands, 2007; Volume 2, p. 179.
2. Murray, H.H. *Industrial Clays Case Study*; No. 64; Mining, Minerals and Sustainable Development: London, UK, 2002.
3. Ekosse, G.E. Fourier transform infrared spectrophotometry and X-ray powder diffractometry as complementary techniques in characterizing clay size fraction of kaolin. *J. Appl. Sci. Environ. Manag.* **2005**, *9*, 43–48. [[CrossRef](#)]

4. López, J.M.G.; Bauluz, B.; Fernández-Nieto, C.; Oliete, A.Y. Factors controlling the trace-element distribution in fine-grained rocks: The Albian kaolinite-rich deposits of the Oliete Basin (NE Spain). *Chem. Geol.* **2005**, *214*, 1–19. [[CrossRef](#)]
5. McLennan, S.M.; Hemming, S.; McDaniel, D.K.; Hanson, G.N. Geochemical approaches to sedimentation, provenance, and tectonics. *Geol. Soc. Am.* **1993**, *284*, 21–40.
6. Jones, B.; Manning, D.A.C. Comparison of geochemical indices used for the interpretation of paleoredox conditions in ancient mudstones. *Chem. Geol.* **1984**, *111*, 111–129. [[CrossRef](#)]
7. Cullers, R.L. The controls on the major- and trace-element evolution of shales, siltstones and sandstones of Ordovician to Tertiary age in the Wet Mountains regions, Colorado, USA. *Chem. Geol.* **1995**, *123*, 107–131. [[CrossRef](#)]
8. Cullers, R.L. The geochemistry of shales, siltstones and sandstones of Pennsylvanian-Permian age, Colorado, USA: Implications for provenance and metamorphic studies. *Lithos* **2000**, *51*, 181–203. [[CrossRef](#)]
9. Armstrong-Altrin, J.S.; Nagarajan, R.; Madhavaraju, J.; Rosalez-Hoz, L.; Lee, Y.I.; Balaram, V.; Cruz-Martínez, A.; Avila-Ramírez, G. Geochemistry of the Jurassic and Upper Cretaceous shales from the Molango Region, Hidalgo, eastern Mexico: Implications for source-area weathering, provenance, and tectonic setting. *C. R. Geosci.* **2013**, *345*, 185–202. [[CrossRef](#)]
10. Nagarajan, R.; Armstrong-Altrin, J.S.; Kessler, F.L.; Hidalgo-Moral, E.L.; Dodge-Wan, D.; Taib, N.I. Provenance and tectonic setting of Miocene siliciclastic sediments, Sibuti formation, northwestern Borneo. *Arab. J. Geosci.* **2015**, *8*, 8549–8656. [[CrossRef](#)]
11. Sheldon, N.D.; Tabor, N.J. Quantitative paleoenvironmental and paleoclimatic reconstruction using paleosols. *Earth-Sci. Rev.* **2009**, *95*, 1–52. [[CrossRef](#)]
12. Sheppard, S.M.F.; Gilg, H.A. Stable isotope geochemistry of clay minerals. *Clay Miner.* **1996**, *31*, 1–24. [[CrossRef](#)]
13. Ekosse, G.E. Thermoanalytical characterization, stable isotopes and paleoenvironmental considerations of kaolinite from two genetic sources. *Fresenius Environ. Bull.* **2008**, *17*, 29–42.
14. Lee, Y.I. Geochemistry of shales of the Upper Cretaceous Hayang Group, SE Korea: Implications for provenance and source weathering at an active continental margin. *Sediment. Geol.* **2009**, *215*, 1–12. [[CrossRef](#)]
15. Fernández-Caliani, J.C.; Gálan, E.; Aparicio, P.; Miras, A.; Márquez, M.G. Origin and geochemical evolution of the Nuevo Montecastelo kaolin deposit (Galicia, NW Spain). *Appl. Clay Sci.* **2010**, *49*, 91–97. [[CrossRef](#)]
16. Clauer, N.; Fallick, A.E.; Gálan, E.; Aparicio, P.; Miras, A.; Fernández-Caliani, J.C.; Aubert, A. Stable isotope constraints on the origin of kaolin deposits from Variscan granitoids of Galicia (NW Spain). *Chem. Geol.* **2015**, *417*, 90–101. [[CrossRef](#)]
17. Gilg, H.A.; Hülmeyer, S.; Miller, H.; Sheppard, S.M.F. Supergene origin of the lastarria kaolin deposit, South-Central Chile, and paleoclimatic implications. *Clays Clay Miner.* **1999**, *47*, 201–211. [[CrossRef](#)]
18. Diko, M.L. Genesis and Ceramic Applications of Selected Kaolin Occurrences from Limpopo Province, South Africa and South West Region. Ph.D. Thesis, University of Limpopo, Polokwane, South Africa, 2011, unpublished.
19. Brandl, G.; Soutpansberg Group. *Catalogue of South African Lithostratigraphic Units*; SA Committee for Stratigraphy, Council Geoscience: Pretoria, South Africa, 2000; pp. 6-39–6-41.
20. Council for Geosciences. *1:250,000 Geological Series*; Sheet 2228 Alldays; Council for Geosciences: Pretoria, South Africa, 2002.
21. Catuneanu, O.; Eriksson, P.J. The sequence stratigraphic concept and the Precambrian rock record: An example from the 2.7–2.1 Ga Transvaal Supergroup, Kaapvaal Craton. *Precambrian Res.* **1999**, *97*, 215–251. [[CrossRef](#)]
22. Eriksson, P.G.; Reczko, B.F.F. The sedimentary and tectonic setting of the Transvaal Supergroup floor rocks to the Bushveld Complex. *J. Afr. Earth Sci.* **1995**, *21*, 487–504. [[CrossRef](#)]
23. Ekosse, G. The Makoro kaolin deposit, southeastern Botswana: Its genesis and possible industrial applications. *Appl. Clay Sci.* **2000**, *16*, 301–320. [[CrossRef](#)]
24. Ekosse, G.E. Provenance of the Kgwakgwe kaolin deposit in southeastern Botswana and its possible utilization. *Appl. Clay Sci.* **2001**, *20*, 137–152. [[CrossRef](#)]
25. Jackson, M.L. (Ed.) *Soil Chemical Analysis—Advanced Course*, 2nd ed.; University of Wisconsin: Madison, WI, USA, 1979; p. 497.

26. Van Reeuwijk, L.P. *Procedures for Soil Analysis*; Technical Paper 9; International Soil Reference and Information Centre: Wageningen, The Netherlands, 2002; p. 100.
27. Jochum, K.P.; Nohl, U.; Herwig, K.; Lammel, E.; Stoll, B.; Hofmann, A.W. GeoReM: A New Geochemical Database for Reference Materials and Isotopic Standards. *Geostand. Geoanal. Res.* **2005**, *29*, 333–338. [[CrossRef](#)]
28. Jochum, K.P.; Weis, U.; Schwager, B.; Stoll, B.; Wilson, S.A.; Haug, G.H.; Andreae, M.O.; Enzweiler, J. Reference Values Following ISO Guidelines for Frequently Requested Rock Reference Materials. *Geostand. Geoanal. Res.* **2016**. [[CrossRef](#)]
29. Borthwick, J.; Harmon, R.S. A note regarding ClF_3 as an alternative to BrF_5 for oxygen isotope analysis. *Geochim. Cosmochim. Acta* **1982**, *46*, 1666–1668. [[CrossRef](#)]
30. Diamond, R.E.; Harris, C. Oxygen and hydrogen isotope composition of Western Cape meteoric water. *S. Afr. J. Sci.* **1997**, *93*, 371–374.
31. Bigeleisen, J.; Perlman, M.L.; Prosser, H.C. Conversion of hydrogenic materials to hydrogen for isotopic analysis. *Anal. Chem.* **1952**, *24*, 1356–1357. [[CrossRef](#)]
32. Raphaelalani, A. Paleoenvironmental Conditions Underpinning Kaolinitisation of Lwamondo and Zebediela Kaolin Deposits. Master's Thesis, University of Venda, Thohoyandou, South Africa, 2017, unpublished.
33. Rudnick, R.L.; Gao, S. Composition of the continental crust. *Treatise Geochem.* **2003**, *3*, 1–64.
34. Nesbitt, H.W.; Markovics, G. Chemical processes affecting alkalis and alkaline earths during continental weathering. *Geochim. Cosmochim. Acta* **1980**, *44*, 1659–1666. [[CrossRef](#)]
35. Wronkiewicz, D.J.; Condie, K.C. Geochemistry of Archean shales from the Witwatersrand Supergroup, South Africa: Source-area weathering and provenance. *Geochim. Cosmochim. Acta* **1987**, *51*, 2401–2416. [[CrossRef](#)]
36. Vidal, P. *Geochimie*; Serie Geoscience 1998; Dunod: Paris, France, 1990.
37. Nyakairu, G.W.A.; Koebel, C.; Kurzweil, H. The Buwambo kaolin deposit in central Uganda: Mineralogical and chemical composition. *Geochem. J.* **2001**, *35*, 245–256. [[CrossRef](#)]
38. Mahjoor, A.S.; Karimi, M.; Rastegarlar, A. Mineralogical and Geochemical Characterisation of Clay Deposits from Soouth Abarkouh District of Clay Deposit (Central Iran) and their Applications. *J. Appl. Sci.* **2009**, *9*, 601–614. [[CrossRef](#)]
39. Zuoping, Z.; Chuanxian, L. The behaviour of rare-earth elements (REE) during weathering of granites in Southern Guangxi, China. *Chin. J. Geochem.* **1995**, *15*, 344–352. [[CrossRef](#)]
40. Garver, J.I.; Royce, P.R.; Smick, T.A. Chromium and nickel in shale of the Taconic foreland: A case study for the provenance of fine-grained sediments with an ultramafic source. *J. Sediment. Res.* **1996**, *66*, 100–106.
41. Ekosse, G.E. Kaolin deposits and occurrences in Africa: Geology, mineralogy and utilization. *Appl. Clay Sci.* **2010**, *50*, 212–236. [[CrossRef](#)]
42. Savin, S.M.; Epstein, S. Oxygen and hydrogen isotope geochemistry of clay minerals. *Geochim. Cosmochim. Acta* **1970**, *4*, 25–42. [[CrossRef](#)]
43. Lawrence, J.R.; Taylor, H.P., Jr. Deuterium and oxygen-18 correlation: Clay minerals and hydroxides in Quaternary soils compared to meteoric waters. *Geochim. Cosmochim. Acta* **1971**, *35*, 993–1003. [[CrossRef](#)]
44. Gilg, H.A.; Sheppard, S.M.F. Hydrogen isotope fractionation between kaolinite and water revised. *Geochim. Cosmochim. Acta* **1996**, *60*, 529–533. [[CrossRef](#)]
45. Gálan, E.; Aparicio, P.; Fernández-Caliani, J.C.; Miras, A.; Márquez, M.G.; Fallick, A.E.; Clauer, N. New insights on mineralogy and genesis of kaolin deposits: The Burela kaolin deposit (Northwestern Spain). *Appl. Clay Sci.* **2016**, *131*, 14–26. [[CrossRef](#)]
46. Dominguez, E.A.; Iglesias, C.; Dondi, M.; Murray, H. Genesis of the La Espingarda kaolin deposit in Patagonia. *Appl. Clay Sci.* **2010**, *47*, 290–302. [[CrossRef](#)]
47. Buhmann, C.; Buhmann, D. Hydrogen-isotope geochemistry of diagenetic clay minerals from Cretaceous Sandstones, Alberta, Canada: Evidence for exchange. *Appl. Geochem.* **1990**, *5*, 657–668.
48. Keller, W.D. Classification of kaolins exemplified by their textures in scan electron micrographs. *Clays Clay Miner.* **1978**, *26*, 1–20. [[CrossRef](#)]
49. Eberl, D.D. Clay minerals formation and transformation in rocks and soils. *Philos. Trans. R. Soc. Lond.* **1984**, *311*, 241–257. [[CrossRef](#)]

